International Conference on Mathematics, Computational Methods & Reactor Physics (M&C 2009)
Saratoga Springs, New York, May 3-7, 2009, on CD-ROM, American Nuclear Society, LaGrange Park, IL (2009)

APPLICATIONS OF MONTE CARLO COMPUTATIONAL FRAMEWORK OF A MEDICAL ACCELERATOR USED FOR RADIATION TREATMENT

Bin Han and X. George Xu*
Nuclear Engineering and Engineering Physics
Rensselaer Polytechnic Institute
Troy, New York
hanb3@rpi.edu; xug2@rpi.edu

Bryan Bednarz
Department of Radiation Oncology
Massachusetts General Hospital and Harvard Medical School
Boston, MA
bbednarz@partners.org

ABSTRACT

This paper summarizes the applications of a detailed Monte Carlo model of the Varian Clinac accelerator for various studies on patient organ doses and accelerator activation during radiation therapy treatments. The modeling and validation of the model were presented. The percentage dose depth curves and the lateral dose profiles of both in-field and out-of-field are in good agreements between the calculation data from the computational frame and the measurement data. One of the applications of this computational frame work is to characterize and quantify the photon activation in high energy medical accelerators. The photon activation map and photo-neutron flux map were generated to estimate the occurring locations of the activations. Most photon activations occur along the beam-line components where the photon flux is the highest. In the contrary, the neutron activations occur everywhere around the accelerator. The other application is to calculate out-of-field organ doses for the radiotherapy treatment. The absorbed organ doses of several IMRT treatments for prostate cancer were simulated with a maximum of 103 μSv/MU to the small intestine. The relationship between the organ doses with the gantry angles was estimated. Treatments for pregnant patient were also simulated and the maximum unshielded fetal dose for mantle treatments was 3.63 μGy /MU. Shielded with 7-cm lead plate, the fetal dose can be reduced by a factor of up to 3. The data and methodology are expected to be useful in the radiation treatment planning, operational health physics, shielding design and retrospective risk assessment.

Key Words: Monte Carlo, accelerator, IMRT, organ dose, activation

1. INTRODUCTION

The goal of radiation therapy is to deliver an optimal amount of radiation dose to the tumor volume while sparing adjacent healthy tissues. For most clinical situations, organs far away from the tumor volume are assumed to receive a small amount of radiation dose. However, it

has long been known that such a relatively low-level of dose outside the treatment volume can potentially lead to the induction of second cancers in patients after radiation treatment[1]. In fact, new treatment delivery techniques often improve the local tumor control at the cost of increasing the scattered and leakage radiation exposure to the patient. As a result, there has been a renewed interest recently in the implication of such second cancers due to Intensity Modulated Radiation Treatment (IMRT) and proton therapy[2-6]. Several domestic and international organizations have addressed this important issue. The National Council on Radiation Protection and Measurement (NCRP) Scientific Committee 1-17 is finalizing a report on "Second cancers and cardiopulmonary effects after radiotherapy." The American Association of Physicist in Medicine (AAPM) organized a symposium on "Secondary cancer risk for emerging radiation treatments" during the 2006 AAPM annual meeting in Orlando, FL and subsequently formed Task Group 158 on "Measurements and calculations of doses outside the treated volume." Also, the International Commission on Radiological Protection (ICRP) organized a task group on the "Evaluation and management of secondary cancer risk in radiation therapy."

Figure 1 illustrates a medical linear accelerator which generates three unintended radiation sources to out-of-field dose: radiation scattered inside the patient, scattered radiation from the accelerator head where the secondary collimators are located, and leakage radiation from other parts of the accelerator. If the energy of the primary beam is high enough (about 10 MeV), secondary neutrons and radioactive isotopes from photonuclear interactions are produced inside the accelerator and will contribute to the out-of-field doses. It has been previously stated that the influence of these sources on out-of-field doses depends on the distance from the field edge[7]. The relative contribution of these sources on the out-of-field photon dose at different distances from the field edge has been investigated using mostly measurements[8-12].

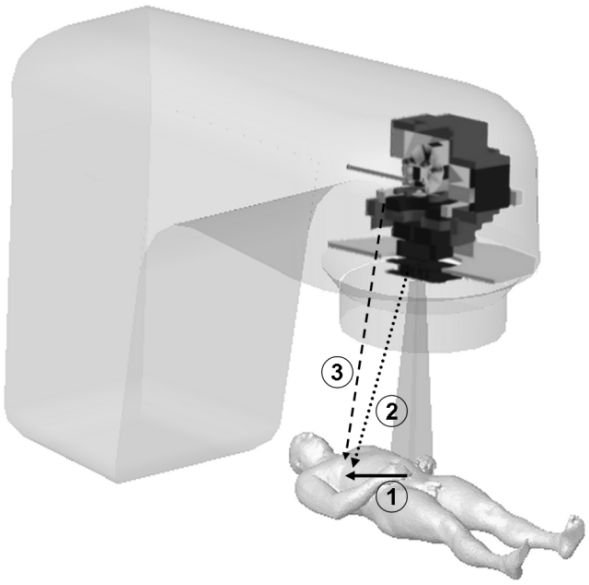

Figure 1: A medical electron accelerator generates out-of-field photon and neutron exposures from three sources (1) patient scatter, (2) secondary collimator scatter, and (3) leakage.

Monte Carlo models of the medical accelerator for scatter and leakage radiation offer a very powerful way to assess out-of-field doses of the patient whose organs are located at various distances from the beam isocenter. However, most existing accelerators models do not consider the detailed shielding components that surround the so-called beam-line components in the accelerator head, and are therefore not sufficient in the study of secondary exposures. The Monte Carlo methods have been widely used[13-14] to simulate the primary radiation treatment fields from medical linear accelerators and calculate in-field (rather than out-of-field) dose distributions. Only the beam-line components—such as the target, primary collimator, flattening filter, jaws, and multi-leaf collimator—were modeled and the out-of-field dose distribution was typically ignored. A few groups have used Monte Carlo methods to simulate the out-of-field dose distributions from medical linear accelerators. Kry et al[15-16] described a method for modeling and validating both 6-MV and 18-MV beams of a Varian Clinac accelerator for out-of-field Monte Carlo dosimetry studies. Both beam-line and secondary shielding were modeled. The secondary shielding includes several components consisting of lead, tungsten, and iron that surround the beam-line components. However, Kry et al did not use of computational patient phantoms that contain well defined organs for either measurement or Monte Carlo calculation. Ideally, a detailed model of the medical accelerator with beam-line components and surrounded shielding components needs to be integrated with whole-body computational phantoms.

This paper summarizes our efforts to develop and to apply a detailed Monte Carlo computational framework consisting of a Varian Clinac medical linear accelerator and various patient phantoms[17]. The necessary shielding surrounding the beam-line components and the patient phantoms are modeled using the Monte Carlo code package MCNPX[18]. The modeling and the validation of the accelerator are presented. The applications of this tool to investigate the photon and neutron activations inside the medical accelerator are discussed. Finally a number of out-of-field organ doses are reported and anaylized.

2. METHODS AND MATERIALS

2.1. The Modeling and Validation of Varian Clinac Accelerator

The beam-line components and an 80-leaf multi-leaf collimator (MLC) were modeled based on the detailed blueprints provided by the vendor. Surrounded shielding geometries and materials were adopted from information provided by Kase et al[19]. Figure 2 illustrates the in-plane plot of the medical accelerator model and labels several beam-line and secondary shielding components shaded in gray. The geometric and material data were defined in the Monte Carlo code package Monte Carlo N-Particle eXtended (MCNPX)[18]. The 6-MV and 18-MV treatment beams were considered for this model. The primary- and secondary-electron tracking is based on the condensed history method. To account for multiple scattering, MCNPX uses an algorithm based on the Goudsmit-Saunderson theory for angular deflections. The Integrated Tiger Series (ITS) indexing method, which has been shown to provide accurate electron dose distributions, was invoked for simulations. The electron and photon cut-off energies were set to

be 0.1 and 0.01 MeV, respectively. In all simulations, variance reduction techniques including geometry splitting, energy cut-offs, and uniform bremsstrahlung splitting were used.

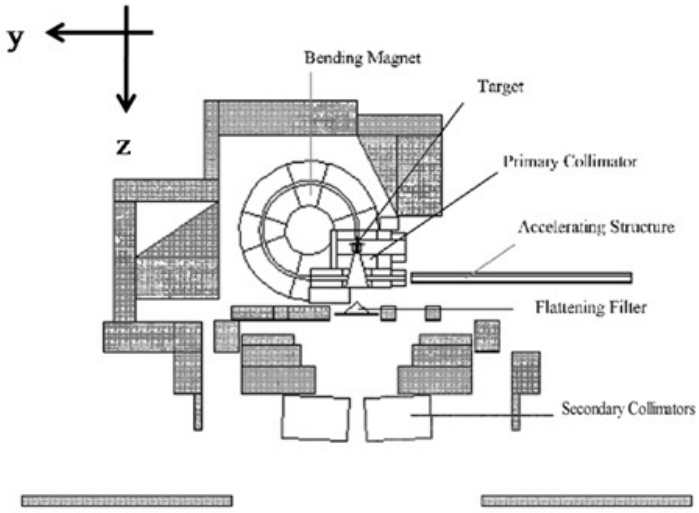

Figure 2. Plot of the Varian Clinac accelerator model using the plotting feature in the MCNPX code. All secondary shielding components are shaded in gray. The MLC was modeled although not plotted here.

2.1.1. In-field validation

In a previous study[17], we performed in-field validation of the accelerator model by calculating the percent depth dose (PDD) and lateral dose profile data for a simulated water phantom with different beam energies and field sizes. We used the type-1 electron "pedep" mesh tally[18] to score the absorbed dose. For both the 6-MV and 18-MV beams, PDDs and lateral dose profiles were generated for 4 cm x 4 cm, 10 cm x 10 cm, and 20 cm x 20 cm field sizes. The lateral dose profiles were calculated at depths of 5, 10, and 20 cm. All results were normalized to the maximum dose, and the calculated PDDs and lateral dose profiles were then compared to measurement data produced by the machines manufacturer. The in-field validation of the accelerator model followed a fine-tuning procedure to optimize the parameters as the mean energy and the incident electron radial intensity distribution to satisfy the pre-defined acceptance criteria. It was determined that for the 6-MV and 18-MV beam the mean energies of the electron beam were 6.2 MeV and 18.3 MeV, respectively. The full-width-half-maximum (FWHM) of the Gaussian spatial spreads of the 6-MV and 18-MV electron beam were 1.3 mm and 1 mm, respectively. For the Gaussian energy distribution of electron-beams, the FWHM was kept constant at 3% of the mean for both 6-MV and 18-MV.

2.1.1. Out-of-field validation

Next, for benchmarking the models for the out-of-field calculations, the photon dose distributions outside the treatment field were simulated and the out-of-field lateral dose profiles were evaluated for different field sizes. To reduce the statistical uncertainty of the calculated

dose in each voxel, the voxel size was set larger than in-field validation. For all simulations the dose recording voxel dimensions were 2 cm in the beam-line direction, 1 cm in the in-plane direction, and 5 cm in the cross-plane direction. It has been previously reported that large voxel sizes are acceptable for out-of-field dose simulations[15-16]. The out-of-field absolute in-plane dose profiles were determined for different field sizes: 4 cm x 4 cm, 10 cm x 10 cm, and 20 cm x 20. All profiles were calculated at a 3.75-cm depth in the water phantom and the dose results were normalized to the maximum dose delivered depending on the specific field size. The calculated profiles were compared to measurement data[15-16].

2.2. Simulations of Photoneutron Yield and Activation Product

High energy photons from medical accelerators produce neutrons and radioactive isotopes from photonuclear interactions in the high-Z accelerator components. To characterize the neutron contamination in the 18-MV Varian Clinac medical accelerator, direct neutron fluences from the accelerator head were calculated in air at various locations using a point detector tally (F5:n). A closed field with both the MLC and jaws fully closed was considered. To quantify the photoneutron yield in all components of the 18-MV accelerator model, the average photon and neutron flux binned by energy were determined using MCNPX. The exact location of each activation event was determined using feature in MCNPX called PTRAC[18].

Three of the dominant activation interactions inside the accelerator head are: photon activations $^{57}Fe(\gamma, p)^{56}Mn$ and $^{65}Cu(\gamma,n)^{64}Cu$; neutron activation $^{186}W(n,\gamma)^{187}W$. To calculate the induced activity, the subsequent photon and neutron activations of the accelerator components were calculated using the average photon and neutron flux convolved with the corresponding IAEA recommended cross section data. The result from the convolution is the activation product yield per source particle. The activation product yields (Y_0) of W^{187}, Cu^{64} and Mn^{56} per monitor unit can be calculated by multiplying a conversion factor (7.86×10^{-16} Gy/electron) of MU to number of source particles, which was determined during the validation process[17]. The equations (1-1) and (1-2) were used to calculate the induced activity during a treatment and the activity buildup during a week.

$$A(t) = Y_0 M (1 - e^{-\lambda t}), \quad t < T \tag{1-1}$$

$$A(t) = Y_0 M (1 - e^{-\lambda T}) e^{-\lambda (t - T)}, \quad t > T \tag{1-2}$$

where A, t, T, Y_0, M, and λ represent the induced activity, time, beam on time, activation product yield per monitor unit (MU), MU delivered rate, and decay constant of certain isotope, respectively.

2.3. Calculations of Out-of-field Organ Doses

The organ doses were calculated using the track-length energy-deposition tally (F6: p) which provided the result that is normalized per source particle. To determine the absolute organ dose from each treatment plan, the dose per source electron in MCNPX was converted to dose per MU. A 6-MV 7-field IMRT treatment and an 18-MV four-field 3D-CRT treatment for prostate

cancer were simulated using RPI Adult Male (RPI-AM) phantom. The absorbed doses from both photon and neutron of fifteen out-of-field organs were calculated.

The radiation protection of the fetus of a pregnant patient during radiation treatment is of particular concern owing to the high radiosensitivity and secondary exposure levels. Xu et al[20] developed RPI P-3, P-6 and P-9 pregnant female (RPI-P) phantom to represent pregnant female at the end of 3-, 6-, and 9-month gestational stages, respectively. Using RPI-P phantoms, several 6-MV mantle field treatments were simulated to calculate the fetal doses. Lead shielding plates with different thicknesses, shapes and locations were then applied to a series of simulations to study the shielding effects.

3. RESULTS AND DISCUSSION

3.1. The Validation of Varian Clinac Accelerator Modeling

The calculated in-field doses were generally in good agreement with measured dose values. Figure 3a shows the PDD curves for the 18-MV beam for the 4 cm x 4 cm, 10 cm x 10 cm, and 20 cm x 20 cm fields. For all doses below the d_{max}, the average local difference between the measured and calculated PDD curves was 1.3%~1.6% for different field sizes. For clarity, The 10 cm x 10 cm field and the 4 cm x 4 cm field were scaled by 80% and 60%, respectively. The 6- and 18-MV lateral dose profiles for the 4 cm x 4 cm, 10 cm x 10 cm, and 20 cm x 20 cm fields were calculated. There is an acceptable agreement between the calculated and measured lateral dose profiles. The average local difference between the calculated and measured dose on the plateau region was within the acceptance criteria of 2%. The average distance between the calculated and measured dose in the penumbra region for all curves were also within the acceptance criteria of 2 mm. For each tally the relative error was less than 2%. Figure 3b shows the 18-MV lateral dose profiles for 10 cm x 10 cm field at depths of 5, 10, and 20 cm. The average local difference between the calculated and measured dose on the plateau region was within the acceptance criteria of 2%.

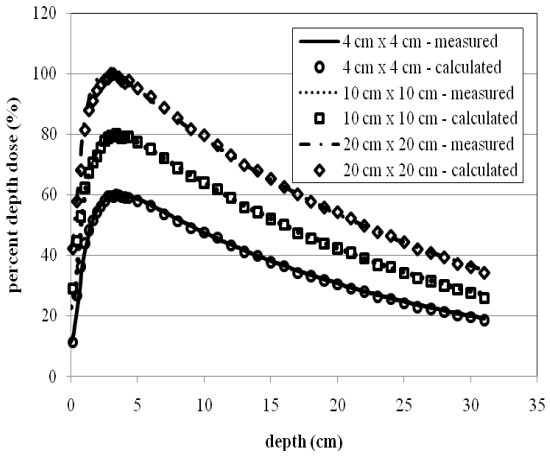

Figure 3a The PDD curves from the 18-MV beam for different field sizes.

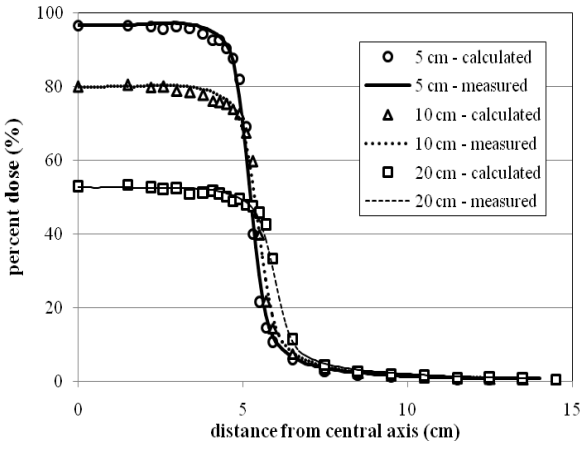

Figure 3b The 18-MV lateral dose profiles for 10 cm x 10 cm field at different depths.

For out-of-field dose validation, there is a good agreement between calculated and measured absolute doses for all field sizes considered. The average difference be calculated and measured absolute dose was 6.2% to 21% for different field sizes and distances less than 60 cm from the isocenter. Figure 4 shows the comparison curves of the measured and calculated out-of-field absolute dose data from the 18-MV beam for field sizes of 5 cm x 5 cm, 10 cm x 10 cm, and 25 cm x 25 cm at a depth of 3.75 cm in an acrylic phantom. The measurement data plotted in the figure was taken from Kry et al[16]. The dose "spike" in the 4 cm x 4 cm dose profiles is due to the effects of the abrupt ending of the MLC in this region. The spike is not seen in larger fields because for these calculations and measurements the MLC was retracted.

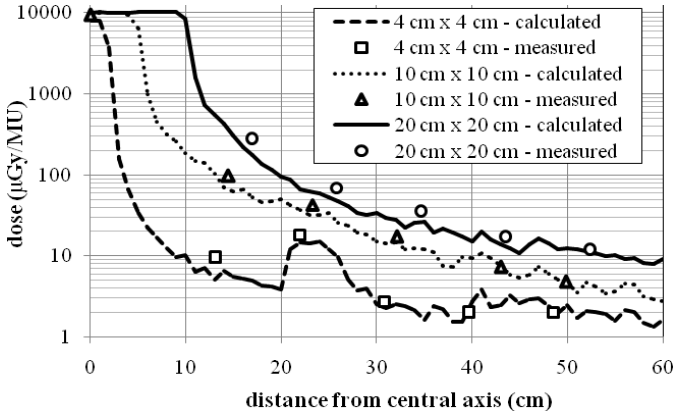

Figure 4 Comparison of measured and calculated out-of-field absolute dose data from the 18-MV beam for field sizes of 5 cm x 5 cm, 10 cm x 10 cm, and 25 cm x 25 cm at a depth of 3.75 cm in the acrylic phantom.

3.2. The Simulation Results of Photoneutron Yield and Activation Product

In a previous study[17], calculated in-air neutron fluences were compared with the calculated and measured neutron fluences by Kry et al[3, 4] and Howell et al[5] and were found to have average differences of 9.5% and 13.7% respectively. The neutron spectrum was calculated and compared with the spectrum provided by Howell et al[5]. The neutron fluence map was generated. The map of the photon activations was also generated. Figure 5 shows the photon activation map for the photo-neutron yield inside the accelerator head. As expected, most photon activations occur along the beam-line components of the accelerator head including the target, primary collimators, secondary collimators, flattening filter, and jaws. That is mainly due to the photon flux along the beam-line components is the highest inside the accelerator head.

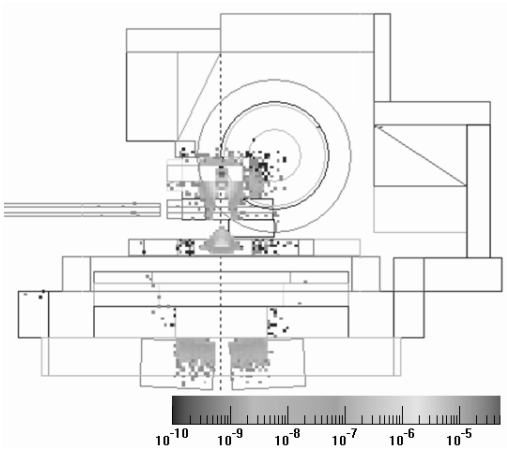

Figure 5 The photon activation map inside the accelerator head

Figure 6 shows the photo-neutron flux around the accelerator head. As can be seen, the photo-neutron flux near the target is the highest on the map. However, unlike the photo activation that occurs dominantly along the beam-line components, the neutrons are found everywhere inside and outside the accelerator head. That means the neutron activation could occur not only inside the accelerator head, but also in the treatment couch, walls and ceiling of the treatment room.

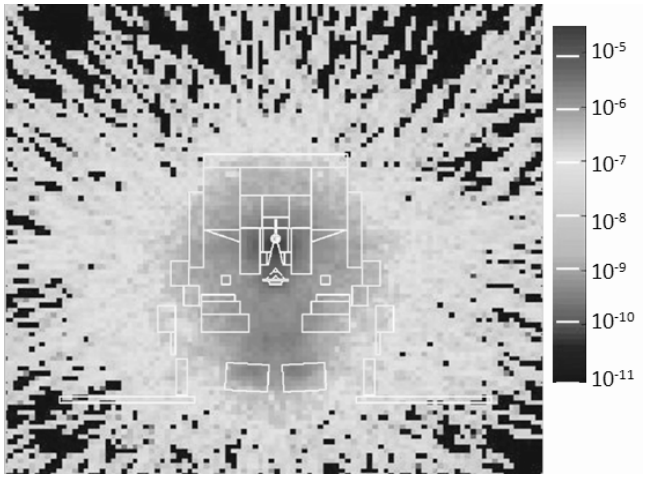

Figure 6 The photo-neutron flux map around the accelerator head

To quantify the photon and neutron activations, induced activities of W^{187}, Cu^{64} and Mn^{56} in all components of the accelerator model were calculated. We assumed each IMRT treatment had an average workload of 700 MU, and each Linac treated 16 patients per day during the weekdays. The radioactivity buildup and decay pattern during a week-long operation was calculated. Figure 7 shows the result of the photon and neutron induced activities inside the accelerator head. The initial radioactivity inside the accelerator was 0 and during the working days it builds up and reaches the highest level in Friday afternoon. Then the induced radioactivity decayed during the weekend where the accelerator is not used.

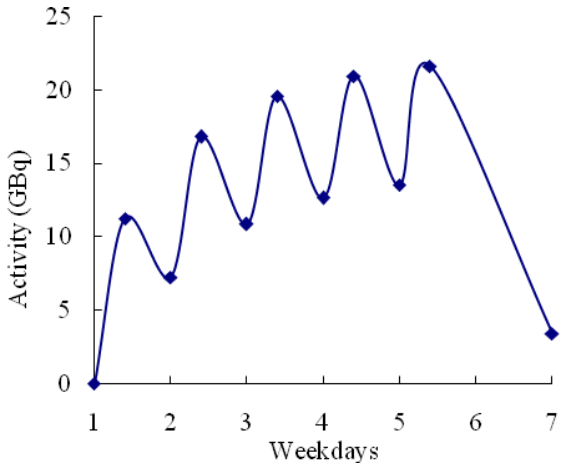

Figure 7 The radioactivity buildup and decay during a week.

3.3. Calculation Results of out-of-field Organ and Fetal Doses

The absorbed doses to 15 organs for 6-MV 7-field IMRT treatment and 18-MV four-field 3D-CRT treatment for prostate cancer were simulated using the accelerator model with RPI-AM phantom. The small intestine received the maximum dose of 103 μSv/MU. The relative errors to all the organ doses were within 10%. The relationship for certain organ doses with gantry angles was estimated.

A series of mantle field radiotherapy treatments to the pregnant patient was also simulated using the RPI P-3 and P-6 pregnant female phantom. The pregnant patient was treated using single beam from the front of the body (AP) with 10 cm x 10 cm field size. The maximum unshielded fetal dose for different mantle treatments was 3.63 μGy /MU. Then, a 7-cm lead shielding plate was added on top of the patient's abdomen. The shielded fetal doses were reduced by a factor up to 3. Figure 8 shows the fetal dose results with and without shielding for different distances from the field edge to the nearest fetus point (DEF). The fetal doses decrease with the increase of the DEF.

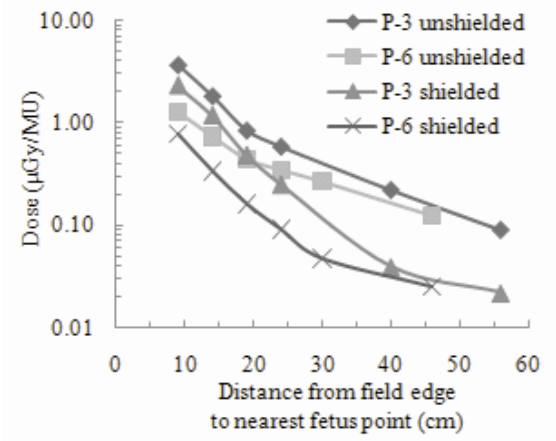

Figure 8 The fetal dose results with and without shielding for different distances from the field edge to the nearest fetus point (DEF).

4. CONCLUSIONS

This paper summarizes the development and applications of a detailed Monte Carlo model of the Varian Clinac accelerator for various studies on accelerator activation and patient organ doses during radiation therapy treatments. To characterize and quantify the photon activation in high energy medical accelerators, the photon activation map and photo-neutron flux map were generated. Most photon activations occur along the beam-line components where the photon flux is the highest, but the neutron activations occur everywhere around the accelerator. Out-of-field organ doses were calculated for the several radiotherapy treatments using RPI-AM phantom. The absorbed doses to 15 organs for several IMRT treatments for prostate cancer were simulated with a maximum of 103 μSv/MU to the small intestine. Treatments for pregnant patient show that the maximum unshielded fetal dose for different mantle treatments was 3.63 μGy /MU. Shielded with 7-cm lead plate, the fetal doses can be reduced by a factor up to 3. The data and methodology presented in this paper demonstrate the usefulness of this Monte Carlo-based computational framework of the medical accelerator for diverse studies involving radiation treatment planning, operational health physics, shielding design and retrospective risk assessment.

ACKNOWLEDGMENTS

The project was supported in part by a grant from the National Cancer Institute (R01CA116743). Mr. Bin Han was a recipient of the Van Auken Research Fellowship from Rensselaer Polytechnic Institute as well as the Robert Gardner Fellowship from the Health Physics Society.

REFERENCES

1. X. G. Xu, B. Bednarz, H. Paganetti, “A review of dosimetry studies on external-beam radiation treatment with respect to second cancer induction” *Phys. Med. Biol.* **53**, pp.R193-R241 (2008)
2. D. Followill, P. Geis, A. Boyer. “Estimates of whole-body dose equivalent produced by beam intensity modulated conformal therapy” *Int. J. Radiat. Oncol. Biol. Phys.* **38**, 667-672 (1997)
3. S. F. Kry, M. Salehpour, D. S. Followill, M. Stovall, D. A. Kuban, R. A. White, I. I. Rosen, “Out-of-field photon and neutron dose equivalents from step-and-shoot intensity-modulated radiation therapy”, *Int. J. Radiat. Oncol. Biol. Phys.* **62**, 1204-1216 (2005)
4. S. F. Kry, M. Salehpour, D. S. Followill, Stovall M. Stovall, D. A. Kuban, R. A. White, I. I. Rosen, “The calculated risk of fatal secondary malignancies from intensity-modulated radiation therapy”, *Int. J. Radiat. Oncol. Biol. Phys.* **62**, 1195-1203 (2005)

5. R. M. Howell et al, "Calculation of effective dose from measurement of secondary neutron spectra and scattered photon dose from dynamic MLC IMRT for 6-MV, 15 MV, and 18-MV beam energies" *Med. Phys.* **33**, pp.360-368 (2006)
6. H. Paganetti, T. Bortfeld, T. F. Delaney,"Neutron dose in proton radiation therapy: in regard to Eric J. Hall" *Int J. Radiat. Oncol. Biol. Phys.* **66**, 1595 (2006)
7. M. Stovall et al, "Fetal dose from radiotherapy with photon beams: Report of AAPM Radiation Therapy Committee Task Group No. 36", *Med. Phys.* **22**, 63-82 (1995)
8. L. Cozzi, F. M. Buffa, A. Fogliata, "Dosimetric features of linac head and phantom scatter radiation outside the clinical photon beam: experimental measurements and comparison with treatment planning system calculations", *Radioth. and Oncol*. **28**, 193-200 (200)
9. Facure A, Da Silva A X, Falcao R C 2007 Monte Carlo simulation of scattered and thermal photoneutron fluences inside a radiotherapy room *Radiat. Prot. Dosim.* **123**, 56-61
10. B. A. Fraass, J. Van de Geijn, "Peripheral dose from megavolt beams", *Med. Phys.* **10**, 809-818 (1983)
11. D.Greene, G. L. Chu, D. W. Thomas, "Dose levels outside radiotherapy beams", *Br. J. Radiol.* **56**, 543-550 (1995)
12. B. Keller, C. Mathewson, P. Rubin, "Scattered radiation doses as a function of x-ray energy", *Radiology* **111**, 447-449 (1974)
13. S. Hartmann, "Description and dosimetric verification of the PEREGRINE Monte Carlo dose calculation system for photon beams incident on a water phantom" *Med. Phys.* **28**, 1322-1337 (2001)
14. D. W. Rogers, B. Walters, I. Kawrakow, "BEAMnrc Users Manual" *NRC Report PIRS* 509(a) (2004)
15. S. F. Kry, U. Titt, F. Ponisch, D. S. Followill, O. N. Vassiliev, R. A. White, R. Mohan, M. Salehpour, "A Monte Carlo model for calculating out-of-field dose from a Varian 6-MV beam" *Med. Phys.* **33**, pp.4405-4413 (2006)
16. S. F. Kry U. Titt, D. S. Followill, O. N. Vassiliev, R. A. White, R. Mohan, M. Salehpour, "A Monte Carlo model for out-of-field dose calculation from high-energy photon therapy" *Med. Phys.* **34**, pp.3489-3499 (2007)
17. B. Bednarz, X. G. Xu, "Monte Carlo modeling of a 6- and 18-MV Varian Clinac medical accelerator for in-field and out-of-field dose calculations: Organ doses from selected treatment plans". Phys. Med. Biol., 54:N43–N57, 2009.
18. Hendricks J. S. et al, *MCNPX Version 2.5.0 LA-UR-04-0569*, Los Alamos, NM (2004)
19. K. R. Kase, G. K. Svensson, A. B. Wolbarst, M. A. Marks, "Measurements of dose from secondary radiation outside a treatment field" *Int. J. Radiat. Oncol. Biol. Phys.* **9**, 1177-1183 (1983)
20. X. G. Xu, V. Taranenko, J. Zhang, C. Shi, "A boundary representation method for designing whole-body radiation dosimetry models: pregnant females at the ends of three gestational periods—RPI-P3, -P6, and -P9", *Phys. Med. Biol.*, **52**, 7023–7044 (2007)